XBPM CALIBRATION AND SIMULATIONS AT SIRIUS

A. G. Oliveira-Filho*, G. Ascenção, S. Luiz, J. Vieira
Brazilian Synchrotron Light Laboratory, Campinas, Brazil

Abstract

X-ray Beam Position Monitors (XBPMs) at SIRIUS/LNLS employ a blade-type design [1] and are not yet fully operational due to ongoing calibration challenges. Minor asymmetries in construction and variations in blade gains can distort the calculated beam position. We applied standard linear-transformation corrections and extended them using a simulated annealing algorithm to optimise the suppression matrix. We also developed a simulation tool that models blade response to radiation for various configurations of blade angles, inter-blade distances, electronic gains, and input beam profiles.

INTRODUCTION

Beam position monitors (BPMs) are an important tool for beam tracking and diagnostics. A common type of device has four sensors that are used to determine the beam position by measuring the field effects on them and then calculating the position using the standard equations for the ratios x_R and y_R,

$$x_R = \frac{(A+D)-(B+C)}{A+B+C+D}, \qquad y_R = \frac{(A+B)-(C+D)}{A+B+C+D}, \tag{1}$$

where A, B, C, and D represent the signals from the sensors (arranged clockwise in a square). The scaled positions, x and y, are then calculated by

$$x = k_x x_R + \delta_x, \qquad y = k_y y_R + \delta_y, \tag{2}$$

where k_x and k_y are the dimensional calibration constants and δ_x and δ_y are the respective offsets. This determination of the beam position is possible in the central region of the device, where the sensors' response is approximately linear.

In the case of an electron beam, which may be considered point-like in a transversal cross-section, Eq. (1) are usually valid in the central region of the BPM. However, in the case of the X-ray beam, the measurement of the beam position may be distorted by its profile, which is relatively large and has a non-uniform intensity distribution. Moreover, minor differences in the construction of the X-ray BPM (XBPM) and variations in the electronic gains of its sensors can amplify these distortions, making the calculated beam position inaccurate.

* arnaldo.filho@lnls.br

XBPM CALIBRATION

We used standard calibration methods to determine the XBPM response, as described by Yang [2] and Chuang *et al.* [3], and then extended these methods by optimizing the transformation matrix using simulated annealing. We also developed a simulation algorithm to model the response of the blades to the incident X-ray radiation, which allows us to calculate the apparent beam position for different configurations of blade angles, inter-blade distances and electronic gains. The simulation accepts a range of input beam profiles, including two-dimensional Gaussian distributions or outputs from radiation transport simulators, and can apply transformations such as stretching and rotation to these profiles.

Standard Calibration Methods

As a calibration method, the XBPM may be displaced to generate a grid of points whose positions are known from the displacement. Beamlines at SIRIUS do not yet have a displacement system for the XBPMs themselves. Alternatively, the calibration was performed by applying orbit bumps to the electron beam at each sector of beamlines with XBPMs, generating such grids [4]. These positions are verified against the beam angles calculated from BPM measurements propagated to the XBPM locations. There are some issues with this approach, however: the bumping process depends on machine study availability, since bumps may interfere with the beam orbit; it is time-consuming for all the XBPMs (the calibration with this method is performed one at a time), and there may be uncertainties associated with wakefields, background noise, and a non-linear trajectory of the electron beam at the source. Nevertheless, the results obtained look consistent with simulations and previous results from the literature [2, 3]. Figure 1 shows the grid of points generated for the Manaca beamline (SIRIUS) as an example. The grid obtained from the XBPM measurements (blue circles in Fig. 1), using Eq. (1), can be compared to the nominal positions (red crosses).

To address these issues, we performed measurements in four SIRIUS beamlines by bumping the electron beam at each corresponding sector and calculating the beam positions with the XBPMs. We followed the procedures described by Chuang *et al.* [3] to apply corrections to the calculated beam position. They consist of applying a linear transformation directly to the signals (A, B, C and D), replacing Eq. (1), before calculating the beam position with Eq. (2). The transformation is calibrated by analyzing the blade behavior along central-symmetry lines, which are the lines where the response of pairs of blades is expected to be equal. Along the central horizontal line, blades A and D are expected to have the same response, as well as blades B and C; along the central vertical line, blades A and B are

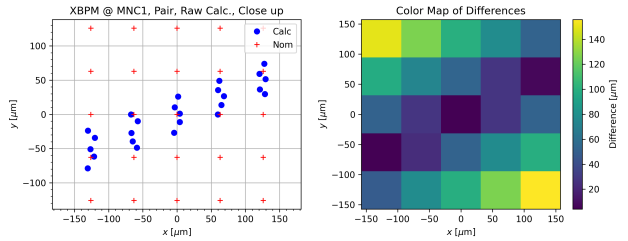

(a) (b)

Figure 1: Grid of points generated for XBPM calibration at Manaca (SIRIUS) beamline. In (a), the positions of the beam are shown at the ROI. Red crosses represent nominal positions, while blue circles represent the positions calculated from the XBPM measurements with Eq. (1). In (b), the mean square error between the calculated and nominal positions is shown. RMS values reach up to 30 µm at the $[-150, 150]$ µm central range (ROI).

expected to have the same response, as well as blades C and D. The slopes of the blade response lines are related to the gain $G_{\lambda,q}$ ($\lambda = A, B, C, D$ and $q = x, y$) of each blade or, reciprocally, the suppression ($s_{\lambda,q} = 1/G_{\lambda,q}$) necessary to correct the signals. We then define the *suppression matrix* $\mathfrak{S}$,

$$\mathfrak{S} = \begin{pmatrix} 1 & -1/G_{B,x} & -1/G_{C,x} & 1/G_{D,x} \\ 1 & 1/G_{B,x} & 1/G_{C,x} & 1/G_{D,x} \\ 1 & 1/G_{B,y} & -1/G_{C,y} & -1/G_{D,y} \\ 1 & 1/G_{B,y} & 1/G_{C,y} & 1/G_{D,y} \end{pmatrix}, \quad (3)$$

$$\mathfrak{S} \cdot \Lambda' = \begin{pmatrix} \Delta x' \\ \Sigma x' \\ \Delta y' \\ \Sigma y' \end{pmatrix} \Rightarrow \begin{pmatrix} x_R \\ y_R \end{pmatrix} = \begin{pmatrix} \frac{\Delta x'}{\Sigma x'} \\ \frac{\Delta y'}{\Sigma y'} \end{pmatrix}. \quad (4)$$

where Λ' is the column vector (A', B', C', D'), which represents the blade signals normalized by the first blade.The first column of $\mathfrak{S}$ is composed of ones because the first blade is used to normalize the others. The physical scaling, Eq. (2), must also be applied to (x_R, y_R). In this case, $k_{x,y}$ and $\delta_{x,y}$ are calculated by fitting the corrected positions to the nominal positions of the grid. The $\Delta_{x,y}$ and the $\Sigma_{x,y}$ are the resulting differences and sums obtained from the product $\mathfrak{S}s$. We developed a software tool to apply these corrections to the calculated beam positions, which is available at [5].

The result of such corrections is shown in Fig. 2, where the calculated positions are much closer to the nominal positions of the grid. The mean square error between the calculated and nominal positions is shown in Fig. 2 (b). Although visually the methods offer a clear improvement, the mean square error is still significant for the desired accuracy.

Simulated Annealing Optimization

We extended these corrections by optimizing the transformation matrix using a simulated annealing algorithm [6]. Starting from the previously calculated suppression matrix, we applied a small variation $\pm\delta$ to the suppressions

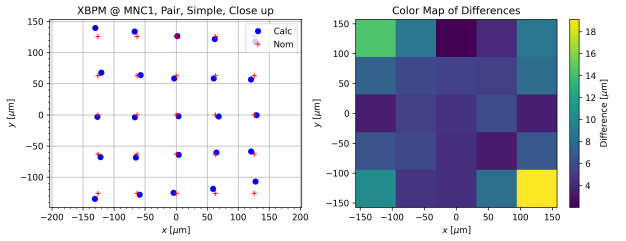

(a) (b)

Figure 2: Grid of points from Fig. 1 corrected by applying Eq. (3) and Eq. (4) at the grid central region (ROI). Figure (a) shows the corrected grid, while Fig. (b) shows the mean square error between the calculated and nominal positions. RMS values reach up to 18 µm at the $[-150, 150]$ µm central range (ROI).

($s_{\Lambda,d} = 1/G_{\Lambda,d}$), one element of $\mathfrak{S}$ at a time, recalculated the beam positions with a refitted scaling and compared the change in RMS error before and after the variation. If the change is negative, the variation is accepted; otherwise, it is accepted with a probability given by the Boltzmann distribution, $p = e^{-\Delta\mathrm{RMS}/T}$, where ΔRMS is the change in RMS and T is a parameter analogous to temperature, which controls the acceptance of negative changes. The algorithm iteratively applies these variations, updating the suppression matrix N times, while gradually decreasing T (the rate of change) and δ (the step size), so that the process is progressively "*cooled down*".

An example of the result of this optimization is shown in Fig. 3, where the calculated positions are even closer to the nominal positions of the grid.

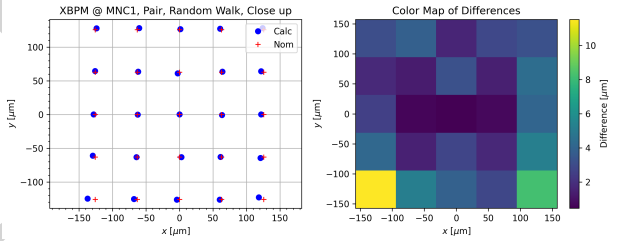

(a) (b)

Figure 3: Grid of points from Fig. 2 corrected by the simulated annealing optimization at the central region (ROI). Figure (a) shows the corrected grid, while Fig. (b) shows the mean square error between the calculated and nominal positions. RMS values were reduced to less than 10 µm at the $[-150, 150]$ µm central range (ROI).

While the optimization process reduced the mean square error for some XBPMs, the measurements from others were too noisy, and the optimization could not provide a definitive calibration. In these cases, the source of instability is still under investigation, but it is believed to be related to the current state of the devices. For beamlines whose source is a dipole (such as Mogno at SIRIUS), the XBPMs measure only the vertical positions, so the vertical scaling works as an optimization by itself; in those cases, the simulated annealing did not provide a significant improvement. The need

for a grid in the calibration of beamlines with ID sources implies a more complex calibration process, which justifies the use of gain analysis and simulated annealing.

SIMULATIONS OF THE XBPM RESPONSE

To deepen our understanding of the relationship between the incident X-ray distribution and the blade geometry, we developed a simulation algorithm to model the response of the blades to incident X-ray radiation [7]. The main purpose was to check the grid configuration when the geometric characteristics of the device and the beam profile are changed. The algorithm calculates the intersection counts of the generated distribution and the region defined by the blades in the two-dimensional section corresponding to the plane of the blades. This allows us to calculate the blade measurements for different configurations of blade angles, inter-blade distances, electronic gains and beam profiles, such as those generated by Gaussian distributions or by radiation transport simulators. The beams may also be stretched or rotated. An example of a beam profile and the intersection can be seen in Fig. 4.

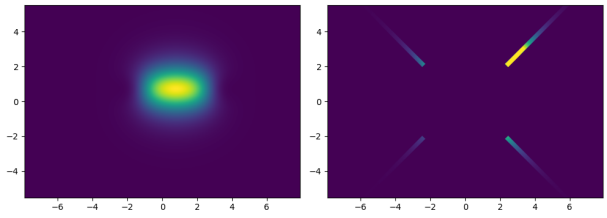

(a) (b)

Figure 4: Example of a beam profile generated by the software SPECTRA [8] (a), simulating the radiation by an APU22, and its intersection with the blades (b). Axes are in millimeters.

The resulting grid of points calculated by the simulation can be seen in Fig. 5. Two configurations of the same beam profile were used, one with its major axes aligned with the *xy* axes, Fig. 5 (a) and (b) (ROI), and another with the beam rotated by 45°, Fig. 5 (c) and (d) (ROI). In Fig. 5 (c) and (d), the grid becomes distorted. Simulations of other changes in the geometry of the system are ongoing, but some preliminary tests with blades at different angles and separation distances show almost no difference in the grid structure. Nevertheless, the general form of the grid with distortions at the borders and the rotation of the grid as a function of the beam profile rotation are consistent with the measurements obtained from the XBPMs, and can explain the observed measurements. Changes in gain for each blade are to be implemented in the simulation as well, so the whole set of experiments might help in understanding what aspects affect the calibration by narrowing down the possible sources of distortion.

CONCLUSION

In this work, we have presented the calibration of the XBPMs at SIRIUS, which is still ongoing. We have applied

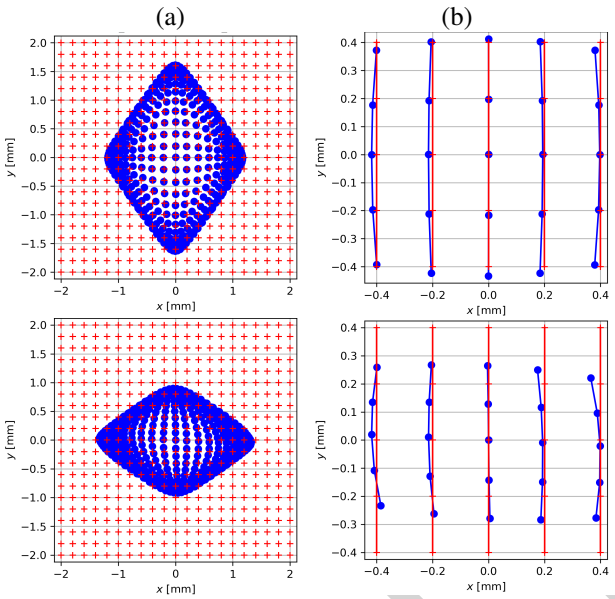

Figure 5: Example of grids resultant from the simulation of a beam profile generated by an APU22 (SPECTRA [8]) intersecting the blades of an XBPM. In (a), the whole grid from the profile aligned with the *xy* axes and in (b) its ROI; in (c), the profile with the beam profile rotated by 45° and in (d), the corresponding ROI.

standard methods to correct the calculated beam position and extended these methods by optimizing the transformation matrix using a simulated annealing algorithm. We have also developed a simulation algorithm to model the response of the blades to the incident X-ray radiation for different geometrical configurations of the device and beam profiles. The results obtained from the simulations are consistent with the measurements, showing that the simulation can be a helpful tool for the calibration process.

REFERENCES

[1] N. Hubert *et al.*, "Design of a New Blade-Type XBPM", in *Proc. IBIC'14*, Monterey, CA, USA, Sep. 2014, paper WEPD22, pp. 687–690.

[2] B. X. Yang *et al.*, "Design and Development for the Next Generation X-ray Beam Position Monitor System at the APS", in *Proc. IPAC'15*, Richmond, VA, USA, May 2015, pp. 1175–1177. doi:10.18429/JACoW-IPAC2015-MOPWI014

[3] J.-Y. Chuang *et al.*, "Discussion and improvement of a blade-type XBPM with coupling suppression by compensating calibration coefficients,"*Nucl. Instrum. Methods Phys. Res., Sect. A*, vol. 953, p. 163174, Feb. 2020. doi:10.1016/j.nima.2019.163174

[4] G. R. Ascenção, "Xbpm measurements from bumps in the electron beam", 2025. https://github.com/lnls-ids/machine-study-scripts/tree/master/xbpms_measurements

[5] A. G. Oliveira-Filho, "Xbpm calibration and analysis at sirius", 2025. https://github.com/lnls-ids/XBPM-bumps

[6] A. G. Oliveira-Filho, "Simulated annealing for XBPM calibration", 2025. https://github.com/lnls-ids/xbpm-randmat

[7] A. G. Oliveira-Filho, "XBPM geoemetry simulations", 2025. https://github.com/lnls-ids/xbpm_sim

[8] T. Tanaka, "Major upgrade of the synchrotron radiation calculation code SPECTRA,"*J. Synchrotron Radiat.*, vol. 28, no. 4, pp. 1267–1272, Jun. 2021. doi:10.1107/s1600577521004100